Communication

Optical Encoding Model based on Orbital Angular Momentum powered by Machine Learning

Erick Lamilla *, Christian Sacarelo, Manuel S. Alvarez-Alvarado, Arturo Pazmino, Peter Iza

Posted Date: 31 January 2023

doi: 10.20944/preprints202301.0573.v1

Keywords: Machine Learning; LG-beams; OAM-beams; Optical Encoding Model

Communication

Optical Encoding Model Based on Orbital Angular Momentum Powered by Machine Learning

Erick Lamilla [1,2,*], Christian Sacarelo [1], Manuel S. Alvarez-Alvarado [3], Arturo Pazmino [1] and Peter Iza [1,4]

[1] Escuela Superior Politécnica del Litoral, ESPOL, Departamento de Física, Campus Gustavo Galindo km 30.5 Vía Perimetral, P.O. Box 09-01-5863, Guayaquil, Ecuador; ealamill@espol.edu.ec
[2] Facultad de Ciencias Matemáticas y Físicas, Universidad de Guayaquil, 090514 Guayaquil; erick.lamillaru@ug.edu.ec.
[3] Escuela Superior Politécnica del Litoral, ESPOL, Facultad de Ingeniería en Electricidad y Computación(FIEC), Campus Gustavo Galindo km 30.5 Vía Perimetral, P.O. Box 09-01-5863, Guayaquil, Ecuador
[4] Center of Research and Development in Nanotechnology, CIDNA, Escuela Superior Politécnica del Litoral, ESPOL, Km 30.5 vía Perimetral, Campus G. Galindo,Guayaquil, Ecuador
* Correspondence: ealamill@espol.edu.ec

Abstract: Based on orbital angular momentum (OAM) properties of Laguerre Gaussian beams LG(p, ℓ), a robust optical encoding model for efficient data transmission applications is designed. This paper presents an optical encoding model based on intensity profile generated by a coherent superposition of two OAM-carrying Laguerre-Gaussian modes and Machine-learning detection method. In the encoding process, the intensity profile for data encoding is generated based on selection of p and ℓ indices, while the decoding process is performed using support vector machine (SVM) algorithm. Two different decoding models based on SVM algorithm are tested to verify the robustness of optical encoding model, finding a BER $= 10^{-9}$ for 10.2 dB of signal-to-noise ratio in one of the SVM models.

Keywords: machine learning; LG-beams; OAM-beams; optical encoding model

1. Introduction

Optical beams with orbital angular momentum (OAM) have aroused a growing interest from researchers around the world due to their wavefront helical shape properties that provide a new degree of freedom for exploration of new applications in particle manipulation [1,2], image processing [3,4] and optical communications [5,6]. In this context, optical communications systems have found a possibility of exploring vortex beams properties in multiplexing [7,8] and data encoding [9,10] pathway. Concerning data encoding, OAM states to encode different data symbols is evidenced by Fang *et al.*[11], where OAM holography is performed by OAM selectivity in spatial-frequency domain without a theoretical helical mode index limit. In the area of holographic encryption, Xiao *et al.* [12] propose a two-coding information metasurfaces to achieve OAM-encrypted holography. OAM encoding has also been explored in multicasting links, for instance, Shiyao Fu *et al.* [13] encode digital signals through the OAM free space one-to-many multicasting link. Within the same research line, data coding has also been explored experimentally as demonstrated by Willner *et al.* in [14], where data encoding at 20 Gb/s, using four possible OAM modes, is performed. Optical encoding and multiplexing techniques in OAM channels for highly dispersive media have also been implemented [10], where a novel scattering-matrix-assisted retrieval technique was proposed to demultiplex OAM channels from highly scattered optical fields.

There is a lot of evidence of OAM applications, for instance, in data encoding field in free space and fiber-based transmission channels [15,16], polarization-based [17,18] and intensity and vortices in phase based [19]. However, implementation of an OAM-based encoding system requires overcoming several challenges from the point of view of information medium propagation and system detection

 doi:10.20944/preprints202301.0573.v1

implementation. Due to the nature of information propagation, some effects can be induced in the medium such as absorption, scattering and turbulence, spatial distortion (amplitude and phase), modal coupling, and crosstalk. Some of these effects, as in the case of turbulence and modal crosstalk, have been potentially suppressed in coding and multiplexing systems, through mitigation methods [20], but for the most part, these effects constitute a great challenge [10,21]. Such challenges have captured attention of scientific community to focus their studies on designing more robust and flexible optical encoders and encryptors, based on coding techniques that minimize noise and information distortion, while correctly maximizing the amount of data coded. In this way, the efforts to improve optical encoding systems are reflected in image recognition methods for encoded data, as in the case of [22], where an index modulation is implemented for OAM states with an Uniform scheme Circular Array (OAM-UCA) to build low-intensity parity coding to improve error performance and transmit additional bits of information. Incoherent detection methods have also been implemented for data decoding [23], where an image information transfer method based on petal-like beam lattices for coding is used. In this case, decoding system works directly with the identification of the intensity patterns captured. Another example of image-based is presented in [19] that employs the amplitude and the phase of an optical field into a phase-only hologram to control spatial transverse modes for data-symbol mapping. A similar study can be found in [24] that uses OAM array for free-space communication link encoding/decoding with 625 states. A proposal for OAM light encoding in magnets has also been developed in[25], where the possible sub-wavelength magnetic phenomena induced by a vortex beam and their applications in the generation of topological defects in chiral magnets is discussed. Although the aforementioned studies show the feasibility of encoding systems based on OAM modes, OAM does not increase the amount of information, nor does it exceed the multiple-input multiple-output (MIMO) transmission of current standards in optical communications[6,26]. In fact, the number of spatial modes available for data encoding is limited by space-bandwidth product of a given optical system [26,27]. A solution to this problem is to use all spatial degrees of freedom offered by OAM modes. A commonly used OAM beam for this purpose is a Laguerre-Gaussian (LG) beam [6,16], which provides eigen-modes dependent on both radial (p) and azimuthal (ℓ) indices; being able to use the superposition of modes to increase the number of encoding data in a limited system. On the other hand, a decoding system (which is generally based on image detection and classification) can present strong signal distortion (both in the intensity profile and in the phase distribution) due to optical alignment, turbulence and scattering [28]. Recently, convolutional neural network (CNN) and Machine-learning techniques have been implemented in optical coding systems, as an alternative solution for image detection and classification [29–31]. High-resolution recognition techniques based on deep learning to encode data in spatial modes have already been implemented [32]. The deep learning-based approach has also been used to recover the sparse data from multiplexed OAM channels independent of phase information [33]. Although these studies demonstrate the feasibility of encoding systems based on OAM modes as well as various methods implemented for data decoding, there is still a gap concerning image detection and classification methods in decoding, due to degradation effects that the medium induces in the transmitted signal, which brings the motivation to this research work.

Motivated by previous statements, this paper proposes a comprehensive optical encoding-decoding system based on the intensity profile generated by a coherent superposition of two OAM-carrying Laguerre-gaussian (LG) modes and Machine-learning detection method. In the encoding process, intensity profile for data encoding is generated based on the selection of p and ℓ indices of LG beams, while the decoding process is performed using support vector machine (SVM). Different from other existing encoding systems that require the additional extraction of phase information, this paper proposes novel optical encoder based on the number of spatial modes carrying data symbols increased in a limited optical system. Moreover, the proposed optical encoding model opens a pathway to a stable image detection and classification system based on Machine-Learning that only uses the intensity profile for target modes. As a result, the main contributions of this paper are: (1) a comprehensive design of a coherent optical encoding system based on the superposition of LG

 doi:10.20944/preprints202301.0573.v1

modes carrying OAM that is independent of phase information, and; (2) a robust decoding system based on intensity profile recognition using the Machine-learning SVM method. Section II presents the concept and operating principle of the optical encoder. In section III, the SVM-based decoding method for image recognition and classification is explained in detail. In section IV, a case study for a 4-bit coding system with different types of noise is considered to validate the robustness of the proposed encoder. Finally, Section V and VI exhibit the results and conclusion, respectively.

2. Concept and principle of optical encoding model

The schematic setup of the conceptual art of this proposed optical encoding model is illustrated in Figure 1. At Transmitter side, an optical system based on a Mach-Zehender interferometer is used to generate a coherent combination of two Laguerre-Gaussian (LG) beams carrying orbital angular momentum (OAM). A laser source (LS) provides a coherent fundamental Laguerre-Gaussian (LG00) beam in free space that is launched to a polarization beam splitter (PBS) to control relative power between reference and selector arm. Both arms will go through an OAM generator to convert a fundamental LG($p = 0, \ell = 0$) mode to a higher-order LG(p, ℓ) mode carrying OAM. The reference arm is converted to a LG($p, \ell = 1$) mode (via OAM Generator 1 in Figure 1), while selector arm is converted to a LG(p, ℓ) mode carrying OAM (via OAM Generator 2 in Figure 1). Since the topological charge ℓ and the radial index p at the LG(p, ℓ) selector beam can be properly selected to generate the intensity pattern for optical encoder, this mode index will be the code-key numbers associated with the data-symbol. The reference and selector arms are combined through a beam splitter (BS1) and the intensity profile of this superposition will be the pattern corresponding to an unique data symbol associated with (p, ℓ) combination. After encoding, the transmitted output beam is transferred to a communication channel, in which different noise sources will be added in order to affect the signal. At Receiver side, the received beam is decoded by Machine Learning process using a support vector machine (SVM)-based method for image recognition and classification.

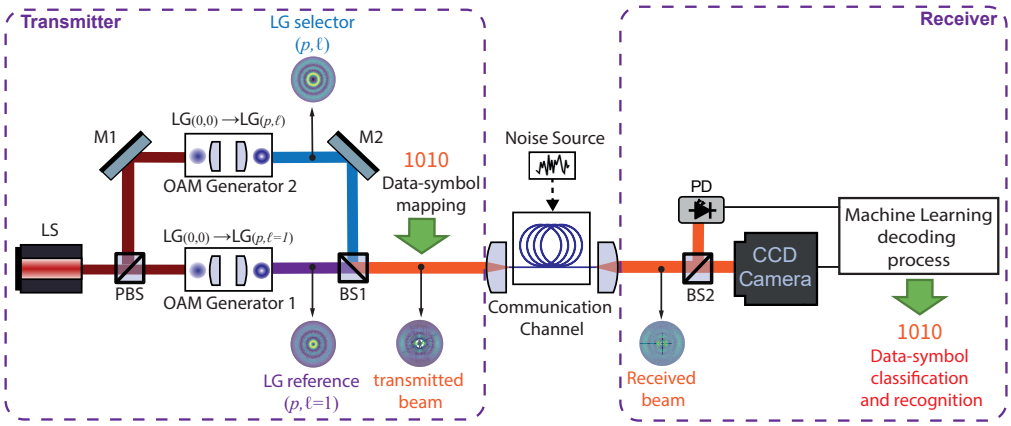

Figure 1. Concept and proposed setup of optical encoding model. LS: laser source; PBS: polarization beam splitter, M1,2: mirror; BS1,2: beam splitter; PD: photodetector.

For generation stage of the intensity pattern that will be used in the transmitter side, the mathematical formulation of the Laguerre-Gaussian beams [34,35] has been used, which are characterized by two indices (p, ℓ) corresponding to radial and azimuthal distribution respectively. The optical field of a LG(p, ℓ) mode can be represented by:

 doi:10.20944/preprints202301.0573.v1

$$
\begin{aligned}
&LG_{p,\ell}(r,\theta,z) \\
&= \sqrt{\frac{2p!}{\pi(p+|\ell|)!}} \frac{1}{w(z)} \left(\frac{r\sqrt{2}}{w(z)}\right)^{|\ell|} L_p^{|\ell|}\left(\frac{2r^2}{w^2(z)}\right) \\
&\exp\left(\frac{-r^2}{w^2(z)}\right) \exp\left(\frac{ik_o r^2 z}{2\left(z^2+z_R^2\right)}\right) \exp(\Phi(z)) \exp(i\ell\theta)
\end{aligned} \tag{1}
$$

where $w(z)$ is the beam width, z_R is the Rayleigh range and $\Phi(z)$ is the Gouy phase. $L_p^{|\ell|}$ are the generalized Laguerre polynomials and (r,θ,z) represents the cylindrical coordinate. Then, the superposition of two LG modes carrying OAM [36] can be expressed as:

$$
u(r,\theta,z) = LG_{p',\ell'}(r,\theta,z) + LG_{p,\ell}(r,\theta,z) \tag{2}
$$

The first term in Eq. 2 describes the reference field, while the second term represents the optical field that acts as a selector. As mentioned, for the optical encoder presented in this work, the $LG(p,\ell = 1)$ mode will be used as the $LG_{p',\ell'}(r,\theta,z)$ reference beam, while the selector beam $LG_{p,\ell}(r,\theta,z)$ will be a previously selected $LG_{p,\ell}$ mode. The same radial index p has been chosen for both reference and selector beam in order to simplify the design of the encoder. Intensity profile of $u(r,\theta,z)$ is associated with a data-bit sequence according to the (p,ℓ) parameters used in the selector beam generation. Since OAM beams have twisted helical phase fronts while propagating, often characterized by the azimuthal index ℓ (also named topological charge) [10], the intensity profile will be most affected in rotations along the propagation axis, without significant changes in the intensity pattern. Additionally, the property of orthogonality between LG modes allows the resulting intensity pattern to be unique for each data symbol [37].

3. SVM- based decoding method for image recognition and classification

The proposed optical encoding model takes as input a 4-bit code defined by the variable X. In addition, a signal noise ratio (SNR) is used to emulate the noise in the communication channel that is given in decibels. The encoding starts with the definition of the variables ℓ_1, ℓ_2 and p to stablish the intensity profile, which is executed by the function *selectCode*. Then, two different intensity profiles are generated using the mathematical formulation given in Eq. 1 and Eq. 2 and declared in $functionLG$. This is followed by the representation of the intensity profile in terms of cartesian coordinates x, y, and the intensity of the resulting beam profile declared in variable I. Next, with a view to emulate a real communication, signal noise is added to the transmitted intensity profile stated in the function addNoise. Later, the *extractHOGFeaturesFromIntensity* function is used to extract useful patterns for information recognition through Histogram of Oriented Gradients (HOG) detection [13]. Finally, the function *predict*, which is based on a linear regression model, is used as a 4-bit classifier through multiclass error-correcting output codes (ECOC) model using support vector machine (SVM) binary learners. For more details about the followed process, the Algorithm 1 is presented. As the process involve training procedures, the decoding processing at the receiver side of the encoder is based on SVM. More details on this SVM algorithm can be found in supplementary material.

 doi:10.20944/preprints202301.0573.v1

Algorithm 1 Pseudocode for decoding processing using SVM–ECOC model

Input X, SNR
Transmission side:
$[\ell_1, \ell_2, p]$=*selectCode*(X) ▷ *Give* ℓ_1, ℓ_2, *and* p *values according to Code Table*
$[x_1, y_1, z_1] = functionLG(\ell_1, \theta_o = 0, \lambda, z = 0, p)$ ▷ *Generate 1st Intensity Profile accord. Eq.1*
$[x_2, y_2, z_2] = functionLG(\ell_2, \theta_o = 0, \lambda, z = 0, p)$ ▷ *Generate 2nd Intensity Profile accord. Eq.1*
$x \leftarrow x_1$
$y \leftarrow y_1$ ▷ *Generate Value for Cartesian coordinates*
$I \leftarrow z_1 + z_2$ ▷ *Superposition of Intensity Profile accord. Eq.2*
Communication Channel:
$n = addNoise(I, SNR)$ ▷ *Add Noise to the intensity in order to simulate real communication signal*
Receiver Side:
$TestFeatures = extractHOGFeaturesFromIntensity(n)$ ▷ *Extract HOG features for the Intensity profile with noise*
$Y = predict(classifier, testFeatures)$ ▷ *Use model from SVM-ECOC Multiclass Training*
Output Y

4. Case Study

As mentioned in the operating principle of the proposed optical encoding model, each data symbol is mapped to a corresponding $u(r, \theta)$ profile, according to the selected modal indices ℓ and p in the selector beam. Since the reference beam is restricted to $LG(p', \ell' = 1)$ mode, the alphabet for possible data symbols within a discrete-time window can be calculated as $log_2 N$ with $N = n_\ell n_p$, where $n_{\ell,p}$ represents the number of ℓ and p indices used in the selector arm and N represents the different data symbols that can be encoded as N -ary numbers: $0, 1, \ldots (N-1)$ [13]. For validation purposes, a data-symbol code based on a 4-bit data symbol $(N = 16)$ is designed, which is associated with the result intensity profile according to the selection of the (p, ℓ) combination, as shown in Figure 2. This table shows all possible combinations of data symbols, the normalized intensity profiles of the reference, selector, and the transmitted beam for data mapping.

No.	Reference LG(p,ℓ=1)	Selector LG(p,ℓ)	Transmitted profile	Data symbol	No.	Reference LG(p,ℓ=1)	Selector LG(p,ℓ)	Transmitted profile	Data symbol
0	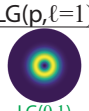 LG(0,1)	 LG(0,1)		**0000**	8	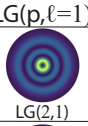 LG(2,1)	 LG(2,1)		**1000**
1	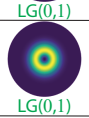 LG(0,1)	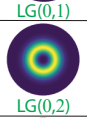 LG(0,2)		**0001**	9	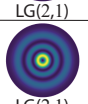 LG(2,1)	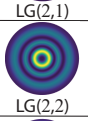 LG(2,2)		**1001**
2	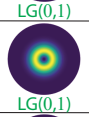 LG(0,1)	 LG(0,3)		**0010**	10	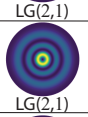 LG(2,1)	 LG(2,3)		**1010**
3	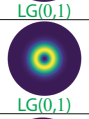 LG(0,1)	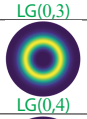 LG(0,4)		**0011**	11	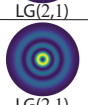 LG(2,1)	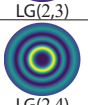 LG(2,4)		**1011**
4	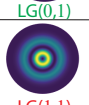 LG(1,1)	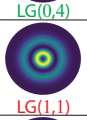 LG(1,1)		**0100**	12	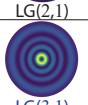 LG(3,1)	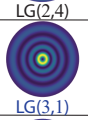 LG(3,1)		**1100**
5	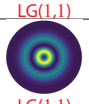 LG(1,1)	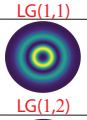 LG(1,2)		**0101**	13	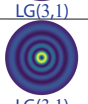 LG(3,1)	 LG(3,2)		**1101**
6	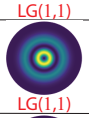 LG(1,1)	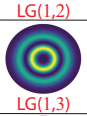 LG(1,3)		**0110**	14	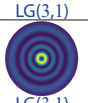 LG(3,1)	LG(3,3)		**1110**
7	LG(1,1)	LG(1,4)		**0111**	15	LG(3,1)	LG(3,4)		**1111**

Figure 2. Data symbol set based on 4-bit data-symbol for the case study presented.

 doi:10.20944/preprints202301.0573.v1

5. Results

The performance of proposed optical encoding model is measured in terms of signal degradation due to addition of noise and Bit Error Rate (BER) presented by the system. It is known that accuracy and precision of an optical encoder depends on detection method and robustness of SVM training algorithm used [38,39]. In this context, to validate the influence of noise on transmission and therefore measure the degree of degradation and signal detection, a combination of RIN and AWGN noises has been used as channel noise for all detection and classification cases. The value of α for RIN has been established by a factor of 0.5 the uniform random distribution, while for AWGN the mean $\mu = 0$ and signal-noise ratio (SNR) levels have been established at 36 dB (low), 30 dB (medium) and 24 dB (high) that are typical noise levels in optical communication systems [40,41].

To understand how the combination of these noises affects the transmitted signal, three different data-symbols are presented in Figure 3; 0011 (Figure 3 a.i), 0110 (Figure 3 b.i) and 1011 (Figure 3 c.i) with their corresponding 2D linear transformations of 200x200 pixels (computational burden), Figure 3 a.ii, b.ii and c.ii. With a view to show the impact of the noises in the transmitted signal, the horizontal position arrangement for pixel 50 of the vertical position (x,50) has been chosen for display purposes, which is presented as a yellow dotted line in the Figure 3 a.ii, b.ii and c.ii. As a result, the normalized intensity curve for such array is presented in Figure 3 a.iii, b.iii and c.iii.

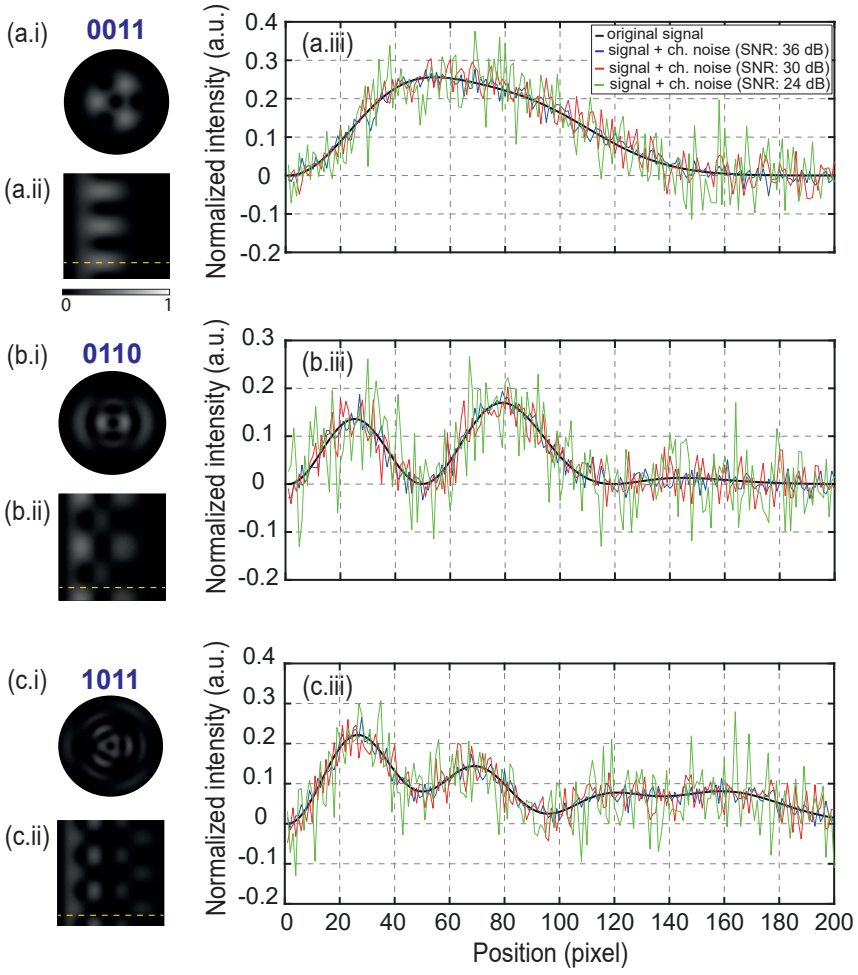

Figure 3. Different data-symbols and their corresponding normalized intensity curves. (a.i) data-symbol 0011, (b.i) data-symbol 0110, (c.i) data-symbol 1011; (a,b,c.ii) Linear transformation of (a,b,c.i); (a,b,c.iii) Normalized intensity curve corresponding to a pixel array of 2D image (dotted yellow line) with different channel noise levels.

 doi:10.20944/preprints202301.0573.v1

The normalized intensity curves show the original transmitted signal in black curve, the received signal with the same α for each case (α = 0.5 for RIN) and with low level channel noise in blue curve, medium level in red curve and high level in green curve. The results of figure 3 reveal that, despite observing distortion in the signal due to addition of noise, for levels greater than 24 dB of SNR, the SVM – ECOC model allows each image to be correctly classified and recognized, with a percentage of 100 % recovery for each data-symbol. For this reason, a computed BER measurement for values less than 24 dB of SNR is necessary to validate the robustness of the optical encoding model at much more critical noise levels.

An end-to-end performance measure for data transmission is BER, which quantifies the reliability of entire coding system from "input bits" to "output bits" including the behaviour of all components and elements between transmitted signal and received signal in addition to considering the path of signal in the middle [42,43]. BER is mathematically defined as the relation between the number of bit-errors and total number of bits [44], which expresses the probability of a bit error. The machine-learning model for prediction, recognition, and classification of images on the receiver side of the proposed optical encoder is based on the SVM–ECOC Multicast algorithm, which can be modelled with binary combinations of each class (one-vs-one) or with binary combinations of one to multiple classes (one-vs-all) [45,46], so the BER measurement for each machine-learning model becomes a reliable metric of confidence level at receiving point. To calculate the BER as a function of SNR at receiver end using the SVM-ECOC model, the training model (one-vs-one or one-vs-all) is first created based on the data set of 4-bit symbols (see Figure 2). Then, the algorithm is trained with 750 images at different SNR levels (from 12 dB to 36 dB in step of 6 dB) in the received signal, to test the functionality of the model at these noise levels. Once the functionality of the SVM model has been verified through the previous training, the images are processed with the model. For image processing, a database consisting of 10000 images for each 4-bit data symbol combination (between 0000 and 1111) was used, resulting in a total of 160000 processed images. The HOG features are extracted from each of these images, to predict the combination of bits corresponding to each image, using the model. Finally, after each prediction, the acquired combination is compared with the original combination and then the BER is calculated. Figure 4 shows the computed BER points as a function of Signal-to-Noise Radio (SNR) from 0 to 14 dB in step of 1 dB for the two proposed SVM-ECOC models: multicast one-vs-one algorithm (model 1) in red curve and Multicast one-vs-all algorithm (model 2) in blue curve.

Since the standard maximum BER for most optical systems is 10^{-9} [47], and for applications in optical communications the maximum BER range is in the range 10^{-9} to $10^{-12)}$ [48], the adjustment curve for each model has also shown in Figure 4 in order to predict noise levels for these values. BER curve for model 1 reaches BER $= 10^{-9}$ for 12.8 dB of SNR (see green line in Figure 4), and BER $= 10^{-12}$ for 13.4 dB of SNR. For the case of model 2 (blue curve in Figure 4) BER $= 10^{-9}$ for 10.2 dB of SNR (see green line in Figure 4), while for a BER $= 10^{-12}$ for 10.9 dB of SNR. Additionally, for comparison purposes, BER estimation curve assuming a probability of error with Gaussian random variable [49] is also shown in black curve. It is observed that, both SVM–ECOC models has a better performance compared to the simplified Gaussian BER model in terms of noise levels, highlighting that, model 2 has a better probability of error compared to model 1, with a difference of 2.65 dB of noise level for BER $= 10^{-9}$. Note that, since the channel noises used in the simulation are AWGN and RIN, the bit errors generated in this case study are directly due to signal degradation by these types of noise. This fact is observed in the results of Figure 4 for each model, indicating that, for an SNR level greater than 9 dB, the bit error probability is below 10 % for model 1 and below 0.0001 % for model 2.

 doi:10.20944/preprints202301.0573.v1

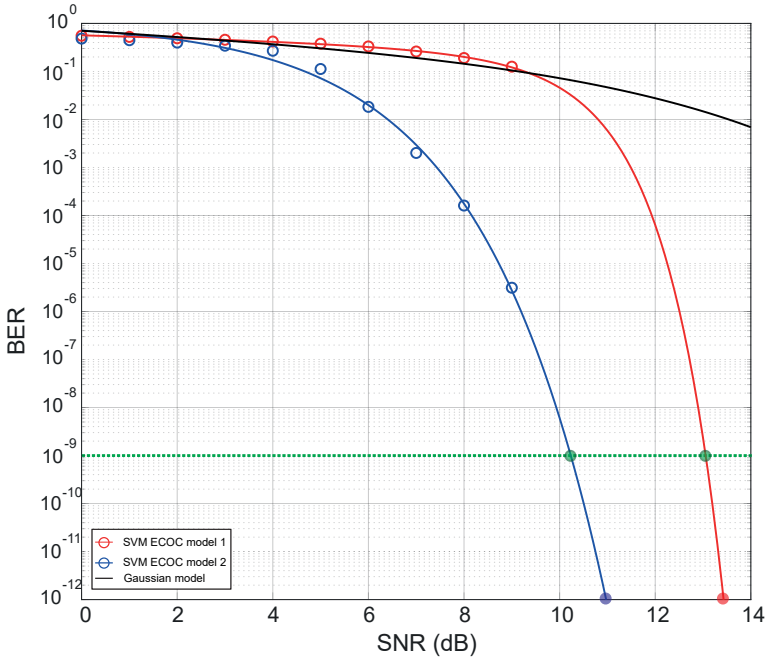

Figure 4. Computed BER for each SVM-ECOC model as a function of SNR for critical noise levels (from 0 to 14 dB).

6. Conclusion

A comprehensive design of an optical encoding model based on the coherent superposition of two *LG* beams with OAM is proposed for the generation of coding system independent of phase information. The proposed approach employs SVM-ECOC algorithm machine learning that enables image prediction, recognition and classification. To verify the robustness of proposed optical encoding model, a data-symbol code based on a 4-bit data symbol is designed, which is associated with the intensity profile according to the (p, ℓ) combination. A channel noise made up of the RIN and AWGN is added to the images generated in encoding stage to emulate a real environment. In order to identify each data-symbol, two different algorithms based on SVM-ECOC model are used. The efficacy of the proposed approach is validated through BER measurements. The results reveal that the proposed algorithms are able to recognize the data-symbol set with a degree of confidence greater than 90 % for noise levels up to 9 dB in both models. Even though both models present high efficiency, the Multicast one-vs-all model (model 2) presents the best BER curve between two models studied, with a BER $= 10^{-9}$ for 10.2 dB of SNR.

For future research, is relevant to mention that the number of circular fringes in the intensity profile of an LG mode are directly related to the index p, while the spatial distribution of these fringes is related to the index ℓ, therefore, the number of bits can be extended to more than 4-bits for the case were $\ell \geq 5$. This fact opens new opportunities for the development of advanced encoding systems.

Author Contributions: Conceptualization, E.L and C.S.; methodology, M.A.; software, C.S.; validation, A.P., E.L. and P.I.; formal analysis, E.L.; investigation, C.S; writing—review and editing, E.L. and M.A. All authors have read and agreed to the published version of the manuscript.

Conflicts of Interest: The authors declare no conflict of interest.

Appendix A. Support Vector Machine Algorithm

As the process involve training procedures, the decoding processing at the receiver side of the encoder is based on Support Vector Machine (SVM). The SVM is a machine learning algorithm that employs the concept of the kernel function to map the data in a different dimensional space, such that the information is grouped according to similar attributes. The algorithm takes as input the raw

 doi:10.20944/preprints202301.0573.v1

data, which is classified depending on the kernel function. Then, the data is saved and compared with the original figure to identify similar patterns that are used for image identification. This process is repeated until the maximum number of iterations n is reached, as shown in Figure A1(a). As a result, a simplification of complex nonlinear decision boundaries is obtained to derive in a linear dimensional space [50]. Mathematically, the characterization is driven by the kernel that can take the form as presented in Table A1. For a better understanding, a flowchart of SVM is presented in Figure A1(b). The kernel used in SVM algorithm for in the proposed optical encoding model is the basis function (Gaussian).

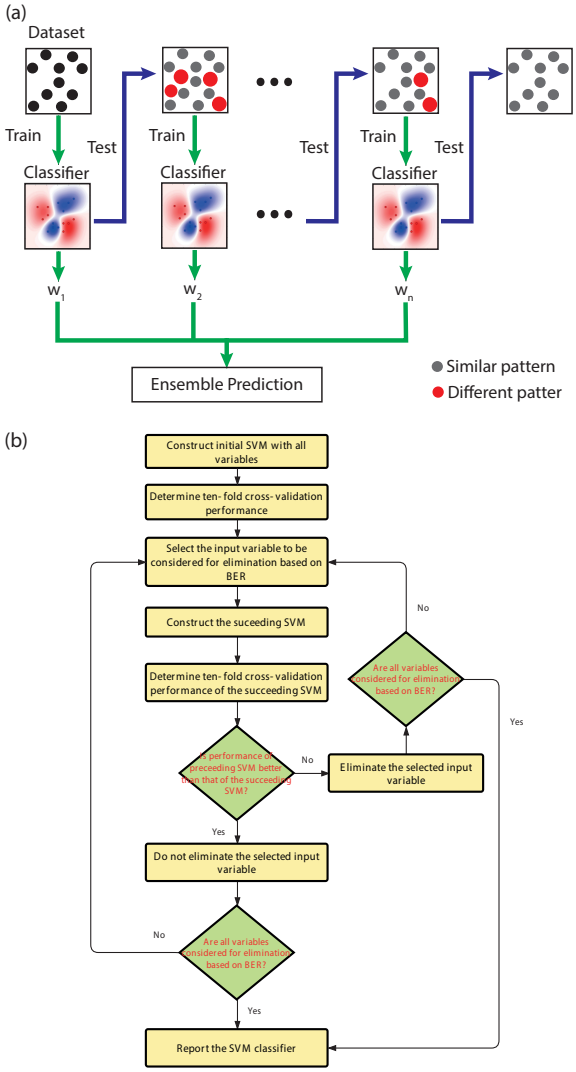

Figure A1. (a) Flow diagram of SVM algorithm. The ensemble classifiers consist of a set of weak classifiers. The weights (wn) of the incorrectly predicted points are increased in the next classifier. The final decision is based on the weighted average of the individual predictions. (b) Flowchart of the application of the Support Vector Machine (SVM) algorithm in the decoding processing.

 doi:10.20944/preprints202301.0573.v1

Table A1. Brief description of the kernels that are used in the different types of SVM algorithms

Type of SVM	Kernel	Description
Base function (Gaussian)	$K(x_1, x_2) = e^{-\frac{\|x_1 - x_2\|^2}{2\sigma^2}}$	Learning of one class, where σ represents the width of the kernel
Linear	$K(x_1, x_2) = x_1^T x_2$	Learning of two classes
Polynomial	$K(x_1, x_2) = (x_1^T x_2 + 1)^\rho$	ρ is the polynomial degree
Sigmoid	$K(x_1, x_2) = \tanh(\beta_0 x_1^T x_2 + \beta_1)$	The kernel is determined by specific β_0 and β_1

References

1. Lian, Y.; Qi, X.; Wang, Y.; Bai, Z.; Wang, Y.; Lu, Z. OAM beam generation in space and its applications: A review. *Optics and Lasers in Engineering* **2022**, *151*, 106923.
2. Zhao, J.; Chremmos, I.D.; Song, D.; Christodoulides, D.N.; Efremidis, N.K.; Chen, Z. Curved singular beams for three-dimensional particle manipulation. *Scientific reports* **2015**, *5*, 1–6.
3. Liu, K.; Cheng, Y.; Gao, Y.; Li, X.; Qin, Y.; Wang, H. Super-resolution radar imaging based on experimental OAM beams. *Applied Physics Letters* **2017**, *110*, 164102.
4. Wang, J.; Liu, K.; Cheng, Y.; Wang, H. Vortex SAR imaging method based on OAM beams design. *IEEE Sensors Journal* **2019**, *19*, 11873–11879.
5. Wang, J. Twisted optical communications using orbital angular momentum. *Science China Physics, Mechanics & Astronomy* **2019**, *62*, 1–21.
6. Trichili, A.; Rosales-Guzmán, C.; Dudley, A.; Ndagano, B.; Ben Salem, A.; Zghal, M.; Forbes, A. Optical communication beyond orbital angular momentum. *Scientific reports* **2016**, *6*, 1–6.
7. Gong, L.; Zhao, Q.; Zhang, H.; Hu, X.Y.; Huang, K.; Yang, J.M.; Li, Y.M. Optical orbital-angular-momentum-multiplexed data transmission under high scattering. *Light: Science & Applications* **2019**, *8*, 1–11.
8. Zhao, Q.; Yu, P.P.; Liu, Y.F.; Wang, Z.Q.; Li, Y.M.; Gong, L. Light field imaging through a single multimode fiber for OAM-multiplexed data transmission. *Applied Physics Letters* **2020**, *116*, 181101.
9. Kai, C.; Feng, Z.; Dedo, M.I.; Huang, P.; Guo, K.; Shen, F.; Gao, J.; Guo, Z. The performances of different OAM encoding systems. *Optics Communications* **2019**, *430*, 151–157.
10. Willner, A.E.; Pang, K.; Song, H.; Zou, K.; Zhou, H. Orbital angular momentum of light for communications. *Applied Physics Reviews* **2021**, *8*, 041312.
11. Fang, X.; Ren, H.; Gu, M. Orbital angular momentum holography for high-security encryption. *Nature Photonics* **2020**, *14*, 102–108.
12. Xiao, Q.; Ma, Q.; Yan, T.; Wu, L.W.; Liu, C.; Wang, Z.X.; Wan, X.; Cheng, Q.; Cui, T.J. Orbital-angular-momentum-encrypted holography based on coding information metasurface. *Advanced Optical Materials* **2021**, *9*, 2002155.
13. Fu, S.; Zhai, Y.; Zhou, H.; Zhang, J.; Wang, T.; Yin, C.; Gao, C. Demonstration of free-space one-to-many multicasting link from orbital angular momentum encoding. *Optics Letters* **2019**, *44*, 4753–4756.
14. Willner, A.J.; Ren, Y.; Xie, G.; Zhao, Z.; Cao, Y.; Li, L.; Ahmed, N.; Wang, Z.; Yan, Y.; Liao, P.; et al. Experimental demonstration of 20 Gbit/s data encoding and 2 ns channel hopping using orbital angular momentum modes. *Optics Letters* **2015**, *40*, 5810–5813.
15. Li, S.; Xu, Z.; Liu, J.; Zhou, N.; Zhao, Y.; Zhu, L.; Xia, F.; Wang, J. Experimental demonstration of free-space optical communications using orbital angular momentum (OAM array encoding/decoding. In Proceedings of the 2015 Conference on Lasers and Electro-Optics (CLEO). IEEE, 2015, pp. 1–2.
16. Trichili, A.; Salem, A.B.; Dudley, A.; Zghal, M.; Forbes, A. Encoding information using Laguerre Gaussian modes over free space turbulence media. *Optics letters* **2016**, *41*, 3086–3089.

17. Wang, J.; Yang, J.Y.; Fazal, I.M.; Ahmed, N.; Yan, Y.; Huang, H.; Ren, Y.; Yue, Y.; Dolinar, S.; Tur, M.; et al. Terabit free-space data transmission employing orbital angular momentum multiplexing. *Nature photonics* **2012**, *6*, 488–496.
18. Zhou, H.; Sain, B.; Wang, Y.; Schlickriede, C.; Zhao, R.; Zhang, X.; Wei, Q.; Li, X.; Huang, L.; Zentgraf, T. Polarization-encrypted orbital angular momentum multiplexed metasurface holography. *ACS nano* **2020**, *14*, 5553–5559.
19. Bolduc, E.; Bent, N.; Santamato, E.; Karimi, E.; Boyd, R.W. Exact solution to simultaneous intensity and phase encryption with a single phase-only hologram. *Optics letters* **2013**, *38*, 3546–3549.
20. Willner, A.E.; Song, H.; Liu, C.; Zhang, R.; Pang, K.; Zhou, H.; Hu, N.; Song, H.; Su, X.; Zhao, Z.; et al. Causes and mitigation of modal crosstalk in OAM multiplexed optical communication links. In *Structured Light for Optical Communication*; Elsevier, 2021; pp. 259–289.
21. Ouyang, X.; Xu, Y.; Xian, M.; Feng, Z.; Zhu, L.; Cao, Y.; Lan, S.; Guan, B.O.; Qiu, C.W.; Gu, M.; et al. Synthetic helical dichroism for six-dimensional optical orbital angular momentum multiplexing. *Nature photonics* **2021**, *15*, 901–907.
22. Zhu, F.; Jiang, J.; Li, Y.; Zhou, C.; Tang, L.; Lai, Z. Index Modulation of OAM-UCA with LDPC Transmission. In Proceedings of the 2021 IEEE 21st International Conference on Communication Technology (ICCT). IEEE, 2021, pp. 1300–1303.
23. Li, Y.; Zhang, Z. Image information transfer with petal-like beam lattices encoding/decoding. *Optics Communications* **2022**, *510*, 127931.
24. Du, J.; Li, S.; Zhao, Y.; Xu, Z.; Zhu, L.; Zhou, P.; Liu, J.; Wang, J. Demonstration of M-ary encoding/decoding using visible-light Bessel beams carrying orbital angular momentum (OAM) for free-space obstruction-free optical communications. In Proceedings of the Optical Fiber Communication Conference. Optica Publishing Group, 2015, pp. M2F–4.
25. Fujita, H.; Sato, M. Encoding orbital angular momentum of light in magnets. *Physical Review B* **2017**, *96*, 060407.
26. Zhao, N.; Li, X.; Li, G.; Kahn, J.M. Capacity limits of spatially multiplexed free-space communication. *Nature photonics* **2015**, *9*, 822–826.
27. Chen, M.; Dholakia, K.; Mazilu, M. Is there an optimal basis to maximise optical information transfer? *Scientific reports* **2016**, *6*, 1–8.
28. Trichili, A.; Park, K.H.; Zghal, M.; Ooi, B.S.; Alouini, M.S. Communicating using spatial mode multiplexing: Potentials, challenges, and perspectives. *IEEE Communications Surveys & Tutorials* **2019**, *21*, 3175–3203.
29. Bartkiewicz, K.; Gneiting, C.; Černoch, A.; Jiráková, K.; Lemr, K.; Nori, F. Experimental kernel-based quantum machine learning in finite feature space. *Scientific Reports* **2020**, *10*, 1–9.
30. Zhou, J.; Huang, B.; Yan, Z.; Bünzli, J.C.G. Emerging role of machine learning in light-matter interaction. *Light: Science & Applications* **2019**, *8*, 1–7.
31. Neary, P.L.; Watnik, A.T.; Judd, K.P.; Lindle, J.R.; Flann, N.S. Machine learning-based signal degradation models for attenuated underwater optical communication OAM beams. *Optics Communications* **2020**, *474*, 126058.
32. Kirchner, T.; Gröhl, J.; Maier-Hein, L. Context encoding enables machine learning-based quantitative photoacoustics. *Journal of biomedical optics* **2018**, *23*, 056008.
33. Zhou, L.; Chen, X.; Chen, W. Deep learning based attack on phase-truncated optical encoding. In Proceedings of the 2020 IEEE MTT-S International Conference on Numerical Electromagnetic and Multiphysics Modeling and Optimization (NEMO). IEEE, 2020, pp. 1–4.
34. Doster, T.; Watnik, A.T. Laguerre–Gauss and Bessel–Gauss beams propagation through turbulence: analysis of channel efficiency. *Applied Optics* **2016**, *55*, 10239–10246.
35. Paufler, W.; Böning, B.; Fritzsche, S. High harmonic generation with Laguerre–Gaussian beams. *Journal of Optics* **2019**, *21*, 094001.
36. Litvin, I.A.; Burger, L.; Forbes, A. Angular self-reconstruction of petal-like beams. *Optics Letters* **2013**, *38*, 3363–3365.
37. Guo, Z.; Wang, Z.; Dedo, M.I.; Guo, K. The orbital angular momentum encoding system with radial indices of Laguerre–Gaussian beam. *IEEE Photonics Journal* **2018**, *10*, 1–11.
38. Zheng, G.; Qian, Z.; Yang, Q.; Wei, C.; Xie, L.; Zhu, Y.; Li, Y. The combination approach of SVM and ECOC for powerful identification and classification of transcription factor. *BMC bioinformatics* **2008**, *9*, 1–8.

39. Liu, M.; Zhang, D.; Chen, S.; Xue, H. Joint binary classifier learning for ECOC-based multi-class classification. *IEEE Transactions on Pattern Analysis and Machine Intelligence* **2015**, *38*, 2335–2341.
40. Binh, L.N. *Noises in optical communications and photonic systems*; CRC Press LLC, 2016.
41. Kareem, F.Q.; Zeebaree, S.; Dino, H.I.; Sadeeq, M.; Rashid, Z.N.; Hasan, D.A.; Sharif, K.H. A survey of optical fiber communications: challenges and processing time influences. *Asian Journal of Research in Computer Science* **2021**, pp. 48–58.
42. Sheng, M.; Jiang, P.; Hu, Q.; Su, Q.; Xie, X.x. End-to-end average BER analysis for multihop free-space optical communications with pointing errors. *Journal of Optics* **2013**, *15*, 055408.
43. Freude, W.; Schmogrow, R.; Nebendahl, B.; Winter, M.; Josten, A.; Hillerkuss, D.; Koenig, S.; Meyer, J.; Dreschmann, M.; Huebner, M.; et al. Quality metrics for optical signals: Eye diagram, Q-factor, OSNR, EVM and BER. In Proceedings of the 2012 14th International Conference on Transparent Optical Networks (ICTON). IEEE, 2012, pp. 1–4.
44. Hayal, M.R.; Yousif, B.B.; Azim, M.A. Performance enhancement of DWDM-FSO optical fiber communication systems based on hybrid modulation techniques under atmospheric turbulence channel. In Proceedings of the Photonics. MDPI, 2021, Vol. 8, p. 464.
45. Hernández, J.A.; Martín, I.; Camarillo, P.; de Arcaute, G.M.R. Applications of Machine Learning Techniques for What-if Analysis and Network Overload Detection. In Proceedings of the 2022 18th International Conference on the Design of Reliable Communication Networks (DRCN). IEEE, 2022, pp. 1–7.
46. Zhang, L.; Li, X.; Tang, Y.; Xin, J.; Huang, S. A survey on QoT prediction using machine learning in optical networks. *Optical Fiber Technology* **2022**, *68*, 102804.
47. Walsh, D.; Moodie, D.; Mauchline, I.; Conner, S.; Johnstone, W.; Culshaw, B. Practical bit error rate measurements on fibre optic communications links in student teaching laboratories. In Proceedings of the 9th International Conference on Education and Training in Optics and Photonics (ETOP), Marseille, France, Paper ETOP021, 2005.
48. Balsells, J.M.G.; López-González, F.J.; Jurado-Navas, A.; Castillo-Vázquez, M.; Notario, A.P. General closed-form bit-error rate expressions for coded M-distributed atmospheric optical communications. *Optics Letters* **2015**, *40*, 2937–2940.
49. Keiser, G. *Fiber Optic Communications*; Springer, 2021.
50. Cervantes, J.; Garcia-Lamont, F.; Rodriguez, L.; López, A.; Castilla, J.R.; Trueba, A. PSO-based method for SVM classification on skewed data sets. *Neurocomputing* **2017**, *228*, 187–197.